Imaging the near surface with frequency domain waveform inversion

Hussain I. Hammad and Gary Margrave

ABSTRACT

Waveform inversion has been demonstrated to be an effective tool in recovering seismic velocities. We test the capability of frequency domain waveform inversion (FDWI) in resolving locally strong lateral velocity variations of the near surface for surface seismic geometries. To study the effect of these variations on FDWI, we use two models, one with the variations and one without. The modelling and the inversion of the models were carried out using the same approach. The final inversion results of both models are well resolved. The result of this work confirms the effectiveness of waveform inversion in handling the strong velocity variations of the near surface.

INTRODUCTION

Waveform inversion refers to the process of iteratively improving an initial model by matching the observed waveforms with modeled ones (Causse et al., 1999). The early papers of Lailly (1983) and Tarantola (1984) provided an efficient way to perform waveform inversion, namely by efficiently computing the gradient of the misfit function. The gradient was derived by linearizing the inverse problem using the first order Born approximation. They showed that the gradient can be computed in a way similar to migration.

One of the early attempts to apply waveform inversion to real data is that by Crase et al. (1990). Further developments and more applications to both synthetic and real data followed in the time domain (Zhou et al., 1995) as well as the in frequency domain(Song et al., 1995; Ravaut et al., 2004). The main advantage of the frequency domain approach is the lower computational cost (Pratt and Worthington, 1990). Since waveform inversion using the multiscale approach requires modelling a few discrete frequencies at a time, the frequency domain approach is more computationally efficient than the time domain approach. Frequency domain finite difference (FDFD) modelling, however, requires the inversion of a sparse operator matrix (Pratt, 1990). The inverse is found using direct methods such as LU decomposition in conjunction with other methods such as nested dissection (Štekl and Pratt, 1998).

The efficient side of using direct methods is that the inverse of the operator matrix is inverted only once, and its inverse is used for multiple sources (Marfurt, 1984). Although iterative methods for finding the inverse are preferred, they require a proper preconditioner. Finding a proper preconditioner is still an active area of research, although some progress has been made (Erlangga, 2008). Plessix (2007) applies a preconditioner to iteratively solve the modelling problem in 3D. Another approach to solve the computationally intensive problem in 3D is to use a massively parallel direct solver (Operto et al., 2007).

Different strategies and preconditioning methods were developed to improve the convergence and to mitigate the non-linearity of the inverse problem. Some strategies include the multiscale strategy of inverting low frequencies first and progressively inverting higher

frequencies (Bunks et al., 1995). Windowing the early arrivals or tapering the late arrivals helps improve convergence to the global minimum (Pratt and Worthington, 1990). Other strategies include smoothing the updates or the gradient or filtering the gradient in the wavenumber domain (Sirgue, 2003; Nemeth et al., 1997).

In this paper, we examine waveform inversion for imaging the near surface, especially the abrupt velocity variations of the near surface. For this purpose we create two velocity models; one with those variations and one without. We carry out the modelling and the inversion for both models bye the same general method.

Wavefrom inversion has already been applied on synthetic and real data to image the near surface (Sheng et al., 2006). In this paper we use an approach that differs from that of Sheng et al. (2006) primarily in two ways. The modelling and the inversion are carried out more efficiently in the frequency domain. Also, the preconditioning method we use is by filtering the gradient in the wavenumber domain as opposed to smoothing the models using the mulitscale smoothing procedure (Sirgue, 2003; Nemeth et al., 1997).

We begin by summarizing the theory of FDWI. After that, we describe the models we created, the modelling and the inversion schemes, and lastly we analyze the results.

THEORY

Forward Modelling

The acoustic wave equation used in modelling is:

$$\nabla\left(\frac{1}{\rho(x,z)}\nabla P(x,z,\omega)\right)+\frac{\omega^2}{K(x,z)}P(x,z,\omega)=S(x,z,\omega) \tag{1}$$

where ρ is the density, K is the bulk modulus, P is the wave field and S is the source term.

Finite differences are used to discretize equation (1). The implementation we use is the 9-point mixed grid approach (Jo et al., 1996; Štekl and Pratt, 1998). Equation (1) can be written in matrix form as follows:

$$Gp=s \tag{2}$$

where G is the impedance matrix, p is the wavefield vector, and s is the source vector. A direct method such as LU decomposition is used to invert the G matrix.

Inversion

We describe here the general scheme for inversion. The reader is referred to Tarantola (1984) and Pratt et al. (1998) for more details. The first step of inversion is to calculate synthetic data using an initial model. The initial model is often obtained using travel time tomography. The synthetic data are then subtracted from the observed data:

$$\delta d=d_{obs}-d_{calc}$$

The objective, then, is to minimize the misfit function, which is the L2 norm of the data residuals:

$$\epsilon = \frac{1}{2}\delta d^t \delta d$$

where t, in δd^t, refers to the transpose. The data residuals are backpropagated into the model. The back-propagated wavefiled is then multiplied (in the frequency domain) by the forward propagated wavefield, to form the gradient of the misfit function, $\nabla\epsilon$. This is expressed mathematically as follows:

$$\nabla\epsilon(x,z,\omega) = \frac{1}{2}\sum_s \sum_r Re\{G_s^*(x,z,\omega)G_r^*(x,z,\omega)\delta d\}$$

where G_s is the source Green's function and G_r is the receiver Green's function.

Then, we can update the model, after calculating the step length function, α, using a line search method, for instance. The update formula then becomes:

$$m^{(l+1)} = m^{(l)} - \alpha^{(l)}\nabla\epsilon^{(l)}$$

NEAR SURFACE IMAGING

Modelling

In this section, we examine FDWI capabilities and response in inverting for near surface velocities. For this purpose, we created two velocity models. The first velocity models is shown in Figure 1c, hereafter referred to as model 1.The prominent features in this model are the sinusoidal structure and velocity gradient within the layers.

The second velocity model, hereafter referred to as model 2, is the same as model 1 except that random velocity variations were added to it, Figure 2c. The variations are normally distributed with a mean of 500 m/s and a standard deviation of 200 m/s. The model is then smoothed by a 2 x 2 smoother. Model 2 exhibits some abrupt velocity variations, a general characteristic of the near surface.

The size of the models is 500x100 grid points, where grid spacing is 10 m. Synthetic data were then acquired over these models. The receiver interval is 20 m and the source interval is 25 m. The location of the first source is 115 m from the left side of the model, and the location of the first receiver is 110 m. The depth of the sources and receivers is 11 grid points below the top of the model. The total number of shots is 191, and the number of traces per shot is 240.

We use frequency domain finite differences, which use Equation 1, to generate the synthetic data. The top boundary is a free surface, whereas the others are absorbing. A sponge boundary condition is used for the corners.

A sample time domain shot record, whose location is in the middle of model 1, is shown in Figure 3a. Although the model is relatively simple, the data are very complex. Another shot record in the same location but in model 2 is shown in Figure 3b.

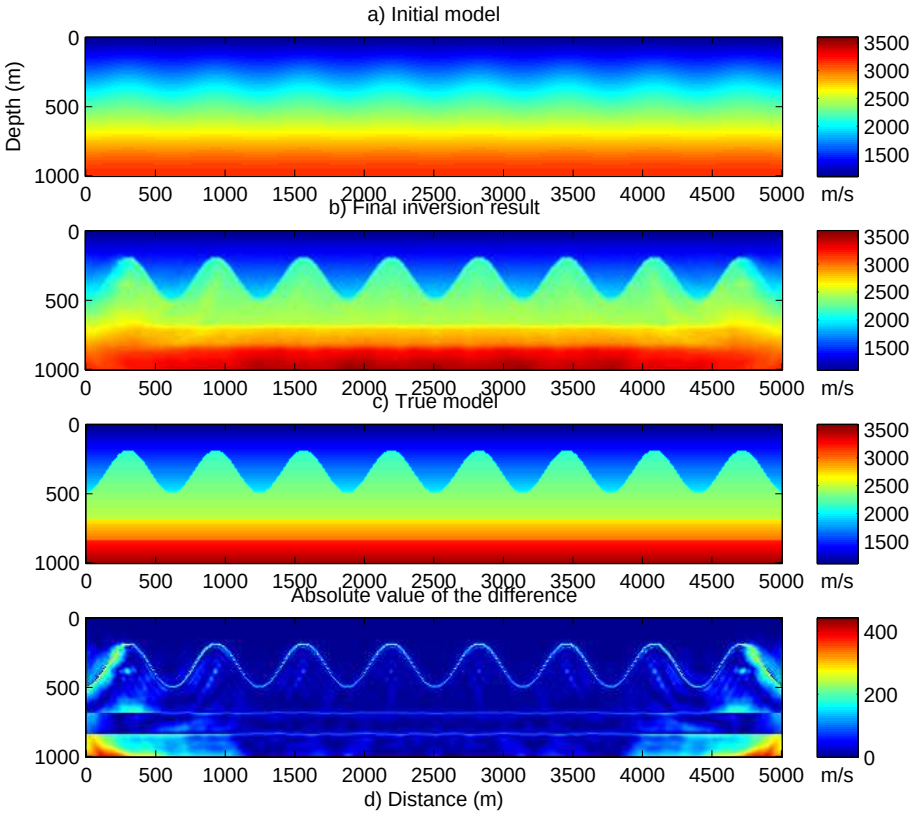

FIG. 1. The velocity models associated with model 1, a-c. D shows the absolute value of the difference between the true model, c, and the estimated model, b.

Since the modelling is done in the frequency domain, the data generated are in the frequency domain as well. Figure 4 and 5 show the real part of the frequency domain panels plotted as surfaces for two frequencies. This representation can be useful in analyzing the data. The affect of the sinusoidal structure of the model is clear for the higher frequency panel in Figure 4, but for the lower frequency it is smoother. This explains why the low frequencies are needed for inversion since they are more sensitive to the low wavenumber component of the model. Since model 2 is more complex than model 1, the effect of the sinusoidal structure is less clear as shown in Figure 5. But the lower frequency panel is still smoother.

Inversion

We started the inversion by creating an initial model for each dataset. The initial models are smoothed versions of the true models. A smoother of 30 x 30 was used. The initial model for model 1 is shown in Figure 1a, whereas that for model 2 is shown in Figure 2a.

After that, we inverted the data using the multiscale strategy, where low frequencies were inverted before the higher frequencies. The lowest frequency component of the data used is 2 Hz, whereas the highest is 24.8 Hz. The number of sequential iterations per frequency are five, and the frequency interval is 0.2 Hz. The inversion could have been more efficient if we used the efficient strategy of Sirgue and Pratt (2004). But this would add

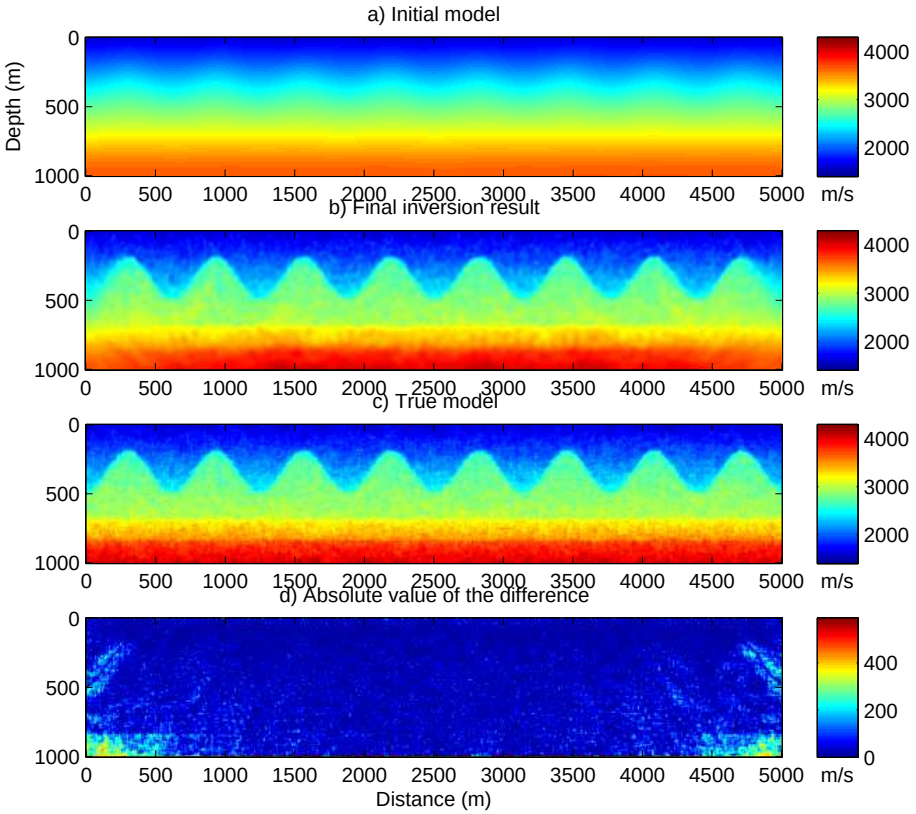

FIG. 2. The velocity models associated with model 2, a-c. D shows the absolute value of the difference between the true model, c, and the estimated model, b.

more complexity to the analysis since more frequencies than the strategy suggests might need to be inverted, as well. The gradient of the misfit function was preconditioned by a low-pass filter in the wavenumber domain (Sirgue, 2003). Although the source signature can be inverted as well, we assumed it to be known in this experiment.

Analysis

The final inversion result of model 1 is shown in Figure 1b. Figure 1d shows the absolute value of the difference between the true and the estimated models. The result is well resolved, as expected, except in some areas. The exact interfaces are not exactly resolved since they are beyond the resolution of the method, which is almost the same as the wavelength (Pratt, 1990). The right and left edges of the model are not resolved to the same degree as the middle part of the model; this is due to incomplete coverage. The same analysis applies to the result of inverting model 2, as shown in Figure 2c and 2d. Because the interfaces are not as well pronounced as in model 1, the inversion result of model 2 is even better resolved at the interfaces. The small velocity variations in model 2, which are beyond the resolution limit, are not completely recovered as shown in Figure 2d.

Figure 6 shows the L2-norm of the difference between the true and the estimated models for each depth. The red curve excludes the left and the right-hand edges of the models since the error is higher in these areas. The blue curve includes all of them. Both figures

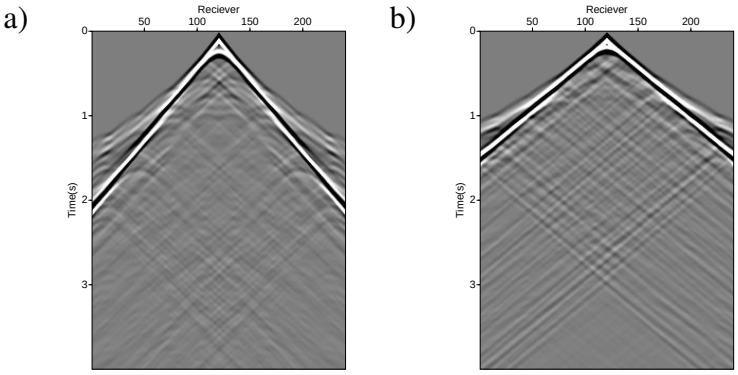

FIG. 3. A sample shot record, a) for model 1 and b) for model 2.

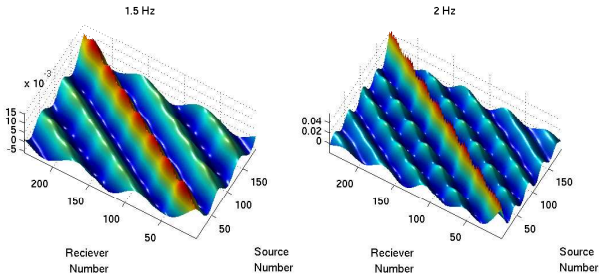

FIG. 4. Frequency domain panels for model 1.

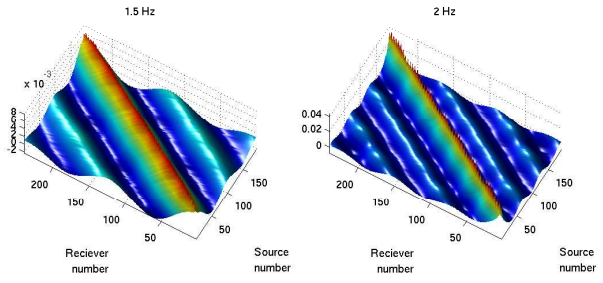

FIG. 5. Frequency domain panels for model 2.

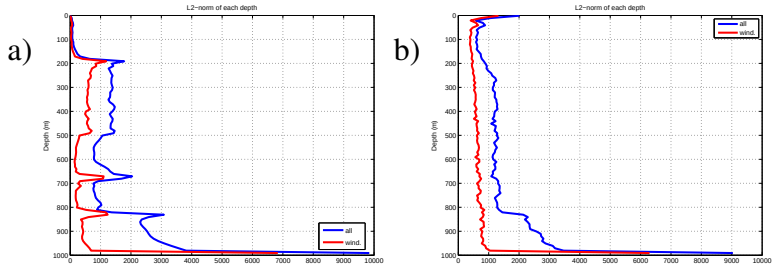

FIG. 6. L2 norm of the difference between the true and the estimate models for each depth. a) for model 1 and b) for model2.

show a general trend. The error increases with depth, as expected. In Figure 6a, the error is particularly high within the sinusoidal structure since it is more complex than the flat layers below. On the other hand, Figure 6b does not exhibit this characteristic clearly, since complexity is randomally distributed in the model. Note that the error is higher on the top part of Figure 6b; this is due to the fact that receivers are lowered into the model.

CONCLUSIONS AND DISCUSSION

FDWI provides an effective and efficient way of imaging the near surface. We showed that even in the presence of locally strong variations of velocity, FDWI is capable of resolving such models. A drawback of waveform inversion is that it requires a good initial model or very low frequencies.

The Blackfoot 2D dataset of CREWES was acquired with low frequencies in mind. Different types of geophones were used, namely 2 Hz, 4.5 Hz and 10 Hz geophones. Applying FDWI to such dataset should answer some questions such as, what types of geophones are more economic and effective.

Although there are many questions to be addressed in waveform inversion, a particularly difficult one is estimating uncertainty. Because the inverse problem is highly nonlinear, error propagation becomes very difficult. In fact, there is presently no proper theory that addresses this problem (Snieder, 1998; Sambridge et al., 2006).

ACKNOWLEDGMENT

We would like to thank the industrial sponsors of CREWES (Consortium for Research in Elastic Wave Exploration Seismology) and POTSI (Pseudodifferential Operator Theory in Seismic Imaging). We also thank MITACS (Mathematics of Information Technology and Complex Systems of Canada) and NSERC (Natural Sciences and Engineering Research Council of Canada). The first author is supported by Saudi Aramco. We used OMEGA and FULLWV by R. Gerhard Pratt and others. We also used Seismic Unix.

REFERENCES

Bunks, C., Saleck, F. M., Zaleski, S., and Chavent, G., 1995, Multiscale seismic waveform inversion: Geophysics, **60**, No. 5, 1457–1473.

Causse, E., Mittet, R., and rn Ursin, B., 1999, Preconditioning of full-waveform inversion in viscoacoustic

media: Geophysics, **64**, No. 1, 130–145.

Crase, E., Pica, A., Noble, M., McDonald, J., and Tarantola, A., 1990, Robust elastic nonlinear waveform inversion: Application to real data: Geophysics, **55**, No. 5, 527–538.

Erlangga, Y. A., 2008, Advances in iterative methods and preconditioners for the helmholtz equation: Archives of Computational Methods in Engineering, **15**, No. 1, 37–66.

Jo, C.-H., Shin, C., and Suh, J. H., 1996, An optimal 9-point, finite-difference, frequency-space, 2-d scalar wave extrapolator: Geophysics, **61**, No. 2, 529–537.

Lailly, P., 1983, The seismic inverse problem as a sequence of before stack migrations, 206Ű220.

Marfurt, K. J., 1984, Accuracy of finite-difference and finite-element modeling of the scalar and elastic wave equations: Geophysics, **49**, No. 5, 533–549.

Nemeth, T., Normark, E., and Qin, F., 1997, Dynamic smoothing in crosswell traveltime tomography: Geophysics, **62**, No. 1, 168–176.

Operto, S., Virieux, J., Amestoy, P., L'Excellent, J.-Y., Giraud, L., and Ali, H. B. H., 2007, 3d finite-difference frequency-domain modeling of visco-acoustic wave propagation using a massively parallel direct solver: A feasibility study: Geophysics, **72**, No. 5, SM195–SM211.

Plessix, R.-E., 2007, A helmholtz iterative solver for 3d seismic-imaging problems: Geophysics, **72**, No. 5, SM185–SM194.

Pratt, G., Shin, C., and Hicks, 1998, Gauss-newton and full newton methods in frequency-space seismic waveform inversion: Geophysical Journal International, **133**, No. 2, 341–362.

Pratt, R. G., 1990, Frequency-domain elastic wave modeling by finite differences: A tool for crosshole seismic imaging: Geophysics, **55**, No. 5, 626–632.

Pratt, R. G., and Worthington, M. H., 1990, Inverse theory applied to multi-source cross-hole tomography part 1: Acoustic wave-equation method1: Geophysical Prospecting, **38**, No. 3, 287–310.

Ravaut, C., Operto, S., Improta, L., Virieux, J., Herrero, A., and Dell'Aversana, P., 2004, Multiscale imaging of complex structures from multifold wide-aperture seismic data by frequency-domain full-waveform tomography: application to a thrust belt: Geophysical Journal International, **159**, No. 3, 1032–1056.

Sambridge, M., Beghein, C., Simons, F. J., and Snieder, R., 2006, How do we understand and visualize uncertainty?: The Leading Edge, **25**, No. 5, 542–546.

Sheng, J., Leeds, A., Buddensiek, M., and Schuster, G. T., 2006, Early arrival waveform tomography on near-surface refraction data: Geophysics, **71**, No. 4, U47–U57.

Sirgue, L., 2003, Inversion de la forme dónde dans le domaine frequential de donnees sismiques grands offsets.: Ph.D. thesis, lÉcole Normale Superieure de Paris.

Sirgue, L., and Pratt, R. G., 2004, Efficient waveform inversion and imaging: A strategy for selecting temporal frequencies: Geophysics, **69**, No. 1, 231–248.

Snieder, R., 1998, The role of nonlinearity in inverse problems: Inverse Problems, **14**, No. 3, 387–404.

Song, Z.-M., Williamson, P. R., and Pratt, R. G., 1995, Frequency-domain acoustic-wave modeling and inversion of crosshole data: Part ii—inversion method, synthetic experiments and real-data results: Geophysics, **60**, No. 3, 796–809.

Tarantola, A., 1984, Inversion of seismic reflection data in the acoustic approximation: Geophysics, **49**, No. 8, 1259–1266.

Štekl, I., and Pratt, R. G., 1998, Accurate viscoelastic modeling by frequency-domain finite differences using rotated operators: Geophysics, **63**, No. 5, 1779–1794.

Zhou, C., Cai, W., Luo, Y., Schuster, G. T., and Hassanzadeh, S., 1995, Acoustic wave-equation traveltime and waveform inversion of crosshole seismic data: Geophysics, **60**, No. 3, 765–773.